frontiers | Frontiers in Earth Science

ORIGINAL RESEARCH
published: 08 August 2022
doi: 10.3389/feart.2022.950305

# Effect of Volcanic Activity on Hydrocarbon-Forming Organisms in Organic-Rich Shale: A Case Study of Dalong Formation in Northwestern Sichuan Basin, China

*Chuanwen Zhang[1,2,3], Qingqiang Meng[2]*, Xuan Tang[3]*, Zuoyu Sun[4], Qian Pang[5], Dawei Lyu[6], Dongya Zhu[2], Jiayi Liu[2], Jiachun Li[4] and Bin Jiang[1]*

[1]State Key Laboratory of Organic Geochemistry, Guangzhou Institute of Geochemistry, Chinese Academy of Sciences, Guangzhou, China, [2]Sinopec Petroleum Exploration and Development Research Institute, Beijing, China, [3]School of Energy and Resources, China University of Geosciences, Beijing, China, [4]School of Earth Science and Spatial Information, Peking University, Beijing, China, [5]School of Earth Science and Technology, Southwest Petroleum University, Chengdu, China, [6]School of Earth Science and Engineering, Shandong University of Science and Technology, Qingdao, China

OPEN ACCESS

**Edited by:**
*Dongming Zhi, PetroChina, China*

**Reviewed by:**
*Yingkun Fu, University of Alberta, Canada*
*Qi Fu, University of Houston, United States*

***Correspondence:**
*Qingqiang Meng*
*mengqq2004@163.com*
*Xuan Tang*
*tangxuan@cugb.edu.cn*

**Specialty section:**
*This article was submitted to Economic Geology, a section of the journal Frontiers in Earth Science*

**Received:** *22 May 2022*
**Accepted:** *13 June 2022*
**Published:** *08 August 2022*

**Citation:**
*Zhang C, Meng Q, Tang X, Sun Z, Pang Q, Lyu D, Zhu D, Liu J, Li J and Jiang B (2022) Effect of Volcanic Activity on Hydrocarbon-Forming Organisms in Organic-Rich Shale: A Case Study of Dalong Formation in Northwestern Sichuan Basin, China. Front. Earth Sci. 10:950305. doi: 10.3389/feart.2022.950305*

Hydrocarbon-generating material determines the elemental composition and hydrocarbon-generating potential of kerogens in a source rock, and it is the key material basis to control the hydrocarbon-generating capacity of the source rock. Previous studies have shown that many intervals of high-quality source rocks generally contain a varying number of volcanic ash layers. The impact of these volcanic ash layers on the development of high-quality source rocks has attracted extensive attention. However, these studies mainly focused on the development of hydrocarbon-forming organisms and the preservation of organic matters but rarely dealt with the differential development of hydrocarbon-forming organisms between multiple volcanic ash layers. The Permian Dalong Formation in the northwestern Sichuan Basin, China, is a set of high-quality source rocks with multiple volcanic sedimentary layers. To understand the differential development of hydrocarbon-forming organisms between volcanic ash layers, with the Dalong Formation in the Longfeng quarry section, Guangyuan, the Sichuan Basin as an example, this study analyzes the types of hydrocarbon-generating materials of high-quality source rocks of the Dalong Formation and the reasons why volcanic activities affected the growth of hydrocarbon-forming organisms and explores the impact of volcanic activities on the development of different types of hydrocarbon-forming organisms. The results show that the TOC of the Longfeng quarry section is 0.05%–15.46%, with an average of 4.76%, and the average TOC of the Dalong Formation is as high as 5.16%, which belongs to high-quality source rocks. The hydrocarbon-forming organism association in the Dalong Formation source rocks is mainly composed of floating algae and benthic algae and vertically divided into three parts: a few radiolarians and trace fossils occasionally in the lower part; a large number of radiolarians, calcium spheres, and algal debris in the middle part; and mainly foraminifera and gastropods in the upper part. There are 36 volcanic ash layers in the Dalong Formation of the study area. In the process of volcanic activity, the "fertilization" effect of volcanic ash made the nutrient elements in the volcanic ash enter

water, increasing the number of hydrocarbon-forming organisms, causing the differential development of various hydrocarbon-forming organisms, and promoting the formation of reducing water to support the preservation of organic matters. The development of hydrocarbon-forming organisms is controlled by the changes of element types and abundances caused by magmatic properties. The time interval of volcanic activities also has an important impact on the development of hydrocarbon-forming organisms.

**Keywords: volcanic activity, hydrocarbon-forming organism, differential development, Dalong Formation, Guangyuan, Sichuan Basin**

## 1 INTRODUCTION

The generation and evolution of source rocks experience a long and complex process under the control of many factors. Previous studies have shown that high-quality source rocks contain multiple volcanic ash layers, such as the Eagle Ford Formation in the Gulf Coast Basin, U.S. (Dawson et al., 2000; Duggen et al., 2007; Lee et al., 2018), the Qingshankou Formation (Gao et al., 2009) and Yingcheng Formation (Shan et al., 2014) in the Songliao Basin, the Shahejie Formation in the Bohai Bay Basin (Du et al., 2014), the Yanchang Formation in the Ordos Basin (Zhang et al., 2009; Qiu et al., 2010; Liu et al., 2013; Xue et al., 2020), the Wufeng–Longmaxi Formations (Lyu et al., 2020; Qiu et al., 2020) and Dalong Formation in the Sichuan Basin (Pang, 2019), and the Haerjiawu Formation (Li, 2010) and Lucaogou Formation (Wu et al., 2012) in the Santanghu Basin, China. This indicates that the formation of organic-rich source rocks might be strongly affected by volcanic activity.

The Sichuan Basin is an important conventional and unconventional oil and gas province in China (Hu et al, 2021b; Xie et al., 2021). The high-quality source rocks of the Dalong Formation in northwestern Sichuan Basin have a good potential for shale oil and gas exploration and development (Fu et al., 2010). Previous studies and stratigraphic sections revealed the presence of multiple volcanic ash interlayers in the Dalong Formation. Deep fluid activities such as volcanic activity can significantly promote the formation of organic-rich shale and the proliferation of hydrocarbon-forming organisms (Liu et al., 2019a; Liu et al., 2019b; Liu et al., 2022). However, for the Dalong Formation high-quality source rocks, further efforts are needed to clarify the relationship between types of hydrocarbon-generating materials and volcanic ash interlayers. The Dalong Formation was deposited successively the overlying Triassic Feixianguan Formation, and it is also the boundary between Permian and Triassic (Li et al., 2020; Zhou et al., 2021). The study on the relationship between types of

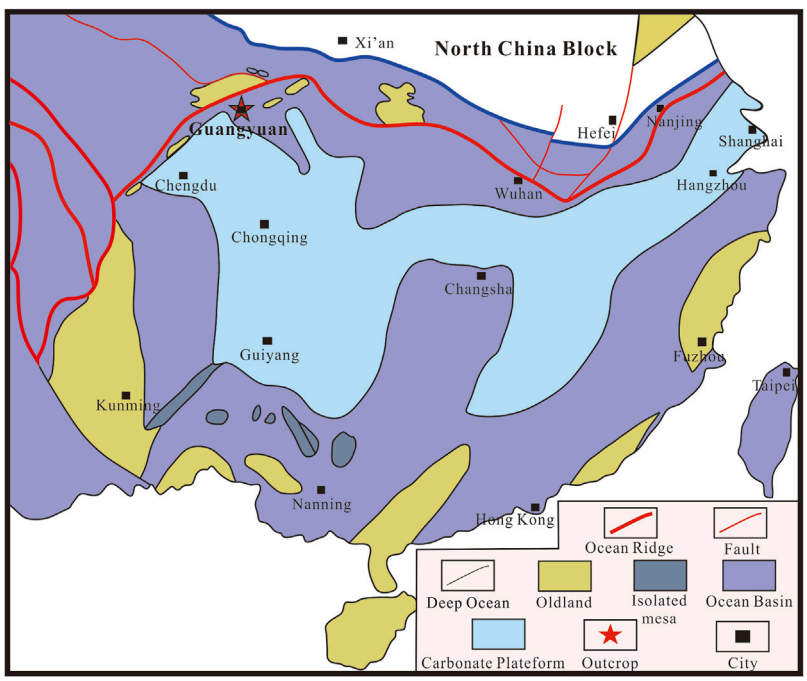


**FIGURE 1 |** Outcrop location (modified after Meng et al., 2022).

**TABLE 1 |** Inorganic elements of Dalong Formation in Longfeng quarry section.

| Sample no. | $Na_2O$ | MgO | $Al_2O_3$ | $SiO_2$ | $K_2O$ | CaO | $TiO_2$ | $Fe_2O_3$ | MoEF | UEF | VEF |
|---|---|---|---|---|---|---|---|---|---|---|---|
| TY-091 | 0.58 | 10.10 | 7.08 | 25.55 | 1.54 | 20.86 | 0.39 | 4.15 | 0.63 | 1.10 | 0.44 |
| TY-090 | 0.62 | 1.72 | 21.84 | 54.00 | 4.17 | 2.78 | 0.53 | 2.31 | 0.31 | 1.05 | 0.38 |
| TY-089 | 0.64 | 1.07 | 12.79 | 67.05 | 2.79 | 3.86a | 0.36 | 2.99 | 1.53 | 0.74 | 0.28 |
| TY-088 | 0.28 | 2.27 | 24.61 | 49.16 | 4.48 | 2.45 | 0.61 | 2.38 | 1.76 | 1.50 | 0.13 |
| TY-087 | 0.35 | 0.81 | 4.58 | 81.24 | 0.99 | 4.70 | 0.17 | 1.15 | 11.88 | 0.98 | 0.53 |
| TY-086 | 0.19 | 0.30 | 2.41 | 68.26 | 0.49 | 14.88 | 0.08 | 0.72 | 12.64 | 3.59 | 0.61 |
| TY-085 | 0.17 | 0.64 | 1.94 | 18.32 | 0.40 | 43.08 | 0.06 | 0.79 | 3.95 | 4.23 | 0.50 |
| TY-084 | 0.28 | 0.59 | 7.33 | 72.28 | 1.69 | 7.01 | 0.25 | 1.73 | 3.00 | 1.48 | 0.43 |
| TY-083 | 0.31 | 2.22 | 2.90 | 35.11 | 0.62 | 30.70 | 0.10 | 1.36 | 3.84 | 5.34 | 0.53 |
| TY-082 | 0.29 | 0.79 | 1.58 | 16.27 | 0.26 | 44.41 | 0.03 | 0.60 | 9.93 | 42.95 | 1.01 |
| TY-081 | 0.36 | 1.27 | 2.16 | 12.56 | 0.40 | 45.51 | 0.08 | 0.87 | 12.67 | 8.81 | 0.59 |
| TY-080 | 0.38 | 0.67 | 2.10 | 10.37 | 0.34 | 47.57 | 0.06 | 1.02 | 8.25 | 13.77 | 0.95 |
| TY-079 | 0.85 | 0.69 | 7.16 | 36.51 | 1.43 | 26.85 | 0.22 | 2.05 | 11.76 | 15.73 | 1.60 |
| TY-078A | 0.26 | 8.02 | 2.81 | 11.85 | 0.61 | 37.02 | 0.10 | 1.68 | 17.60 | 4.96 | 0.63 |
| TY-078 | 0.21 | 1.11 | 0.43 | 1.54 | 0.04 | 53.70 | 0.01 | 0.88 | 35.88 | 36.62 | 0.86 |
| TY-077 | 0.58 | 0.99 | 6.19 | 57.99 | 1.18 | 14.68 | 0.24 | 2.33 | 25.20 | 3.65 | 2.70 |
| TY-076 | 0.75 | 0.62 | 10.18 | 59.78 | 1.86 | 2.98 | 0.32 | 4.43 | 96.64 | 7.41 | 6.90 |
| TY-075 | 0.40 | 2.16 | 3.81 | 57.31 | 0.67 | 16.81 | 0.12 | 1.30 | 37.60 | 4.49 | 1.85 |
| TY-074 | 0.38 | 0.51 | 7.72 | 75.85 | 1.60 | 1.40 | 0.25 | 1.77 | 15.87 | 1.26 | 2.03 |
| TY-073 | 0.26 | 0.84 | 2.86 | 59.29 | 0.54 | 18.73 | 0.08 | 0.65 | 17.31 | 5.00 | 1.23 |
| TY-072 | 0.36 | 0.28 | 2.06 | 69.16 | 0.30 | 14.60 | 0.06 | 0.68 | 25.94 | 18.21 | 1.96 |
| TY-071 | 0.27 | 0.31 | 1.49 | 68.13 | 0.22 | 15.93 | 0.05 | 0.57 | 64.69 | 9.94 | 1.67 |
| TY-070 | 0.40 | 1.31 | 2.33 | 57.06 | 0.32 | 19.31 | 0.06 | 0.64 | 23.69 | 26.33 | 121.52 |
| TY-069 | 0.59 | 0.59 | 3.83 | 71.34 | 0.63 | 10.99 | 0.09 | 0.87 | 41.17 | 3.97 | 51.58 |
| TY-068 | 0.34 | 0.56 | 2.99 | 63.98 | 0.74 | 15.76 | 0.10 | 0.92 | 46.22 | 15.10 | 166.58 |
| TY-067 | 0.33 | 0.55 | 2.14 | 76.61 | 0.32 | 5.55 | 0.08 | 2.43 | 789.72 | 23.47 | 1,015.59 |
| TY-066 | 0.47 | 0.41 | 7.52 | 71.12 | 1.20 | 1.19 | 0.23 | 2.07 | 136.37 | 6.01 | 668.71 |
| TY-065 | 0.22 | 0.21 | 1.29 | 90.89 | 0.22 | 2.18 | 0.04 | 0.92 | 293.10 | 7.14 | 156.94 |
| TY-064 | 0.22 | 0.27 | 3.41 | 82.03 | 0.74 | 2.46 | 0.12 | 1.62 | 331.41 | 5.97 | 584.46 |
| TY-063 | 0.54 | 0.49 | 8.70 | 70.38 | 1.45 | 0.29 | 0.27 | 1.44 | 123.86 | 5.00 | 814.47 |
| TY-062 | 0.32 | 0.45 | 2.74 | 75.62 | 0.55 | 7.53 | 0.10 | 2.66 | 265.27 | 12.83 | 502.25 |
| TY-061 | 0.18 | 0.17 | 1.21 | 83.77 | 0.20 | 4.84 | 0.04 | 1.15 | 709.96 | 67.26 | 461.51 |
| TY-060–1 | 0.27 | 8.69 | 2.86 | 37.71 | 0.73 | 19.41 | 0.12 | 2.22 | 370.31 | 17.75 | 848.90 |
| TY-060 | 0.18 | 0.18 | 1.85 | 80.27 | 0.42 | 3.32 | 0.08 | 1.66 | 895.79 | 18.39 | 633.86 |
| TY-059 | 0.18 | 0.19 | 2.79 | 80.20 | 0.79 | 0.74 | 0.13 | 2.87 | 947.15 | 16.22 | 660.90 |
| TY-058 | 0.45 | 0.19 | 4.38 | 80.58 | 0.92 | 3.82 | 0.15 | 1.31 | 61.47 | 4.25 | 377.26 |
| TY-057–1 | 0.50 | 0.27 | 5.80 | 79.42 | 1.20 | 1.78 | 0.19 | 1.79 | 48.22 | 16.52 | 593.92 |
| TY-057 | 0.58 | 0.46 | 7.97 | 67.01 | 1.62 | 0.22 | 0.29 | 2.95 | 176.94 | 9.62 | 1,695.21 |
| TY-056 | 0.23 | 0.22 | 1.87 | 81.67 | 0.37 | 6.13 | 0.07 | 1.19 | 431.52 | 12.49 | 261.13 |
| TY-055 | 0.20 | 0.88 | 2.59 | 78.22 | 0.55 | 4.45 | 0.10 | 2.41 | 263.88 | 14.29 | 670.35 |
| TY-054 | 0.33 | 0.74 | 3.87 | 72.92 | 0.84 | 3.90 | 0.14 | 2.90 | 387.15 | 11.92 | 967.56 |
| TY-053 | 0.37 | 0.37 | 2.34 | 51.72 | 0.36 | 22.57 | 0.08 | 1.24 | 204.45 | 57.28 | 307.97 |
| TY-052 | 0.63 | 0.68 | 9.88 | 57.45 | 1.92 | 0.10 | 0.42 | 3.01 | 333.74 | 5.30 | 1,397.78 |
| TY-051 | 0.20 | 0.21 | 1.25 | 74.87 | 0.21 | 11.00 | 0.04 | 0.79 | 155.85 | 47.82 | 183.72 |
| TY-050 | 0.13 | 7.92 | 0.50 | 7.19 | 0.07 | 42.62 | 0.02 | 0.29 | 483.96 | 34.53 | 128.27 |
| TY-049 | 0.20 | 1.27 | 2.38 | 79.41 | 0.53 | 3.05 | 0.11 | 1.92 | 393.36 | 10.35 | 713.42 |
| TY-048 | 0.27 | 1.41 | 2.99 | 63.68 | 0.57 | 13.05 | 0.10 | 1.53 | 273.99 | 10.54 | 653.77 |
| TY-047 | 0.14 | 0.24 | 1.77 | 75.40 | 0.33 | 8.66 | 0.06 | 1.51 | 229.17 | 15.49 | 27.86 |
| TY-046 | 0.30 | 0.28 | 3.32 | 71.81 | 0.68 | 6.32 | 0.14 | 2.97 | 313.80 | 12.42 | 15.20 |
| TY-045 | 0.45 | 0.87 | 6.67 | 60.33 | 1.22 | 5.30 | 0.22 | 3.58 | 233.02 | 7.18 | 15.66 |
| TY-044 | 0.49 | 0.87 | 6.10 | 64.18 | 1.16 | 4.38 | 0.22 | 4.65 | 195.53 | 4.38 | 9.75 |
| TY-043–1 | 0.31 | 1.39 | 3.83 | 64.68 | 0.76 | 9.24 | 0.15 | 3.10 | 184.66 | 8.27 | 23.92 |
| TY-043 | 0.20 | 1.25 | 2.10 | 81.18 | 0.41 | 3.78 | 0.09 | 1.43 | 233.58 | 9.08 | 20.61 |
| TY-042 | 0.19 | 9.97 | 2.20 | 36.33 | 0.55 | 20.01 | 0.07 | 1.25 | 273.72 | 12.64 | 17.33 |
| TY-041A | 0.14 | 0.35 | 1.67 | 75.90 | 0.36 | 8.45 | 0.06 | 1.94 | 441.55 | 22.47 | 26.19 |
| TY-041 | 0.45 | 0.61 | 6.50 | 66.63 | 1.25 | 5.01 | 0.21 | 2.35 | 52.17 | 6.47 | 7.19 |
| TY-040A | 0.22 | 0.22 | 1.65 | 84.58 | 0.32 | 3.67 | 0.07 | 0.89 | 113.68 | 14.23 | 13.38 |
| TY-040 | 0.38 | 0.50 | 7.09 | 70.04 | 1.36 | 1.43 | 0.23 | 2.27 | 39.11 | 4.44 | 7.49 |
| TY-039 | 0.23 | 0.86 | 3.52 | 80.92 | 0.85 | 1.70 | 0.14 | 1.26 | 43.24 | 4.17 | 7.39 |
| TY-038 | 0.45 | 0.31 | 5.94 | 63.70 | 1.49 | 0.49 | 0.24 | 6.06 | 309.28 | 6.60 | 24.98 |
| TY-037 | 0.46 | 0.48 | 4.91 | 43.82 | 1.25 | 18.41 | 0.21 | 3.62 | 181.30 | 10.74 | 17.26 |
| TY-036 | 0.43 | 0.57 | 5.60 | 43.80 | 1.54 | 15.34 | 0.23 | 5.02 | 234.97 | 8.56 | 22.73 |
| TY-035 | 0.73 | 9.77 | 5.89 | 15.40 | 0.87 | 29.52 | 0.11 | 1.26 | 12.60 | 5.78 | 3.17 |

(Continued on following page)

**TABLE 1 |** (*Continued*) Inorganic elements of Dalong Formation in Longfeng quarry section.

| Sample no. | $Na_2O$ | MgO | $Al_2O_3$ | $SiO_2$ | $K_2O$ | CaO | $TiO_2$ | $Fe_2O_3$ | MoEF | UEF | VEF |
|---|---|---|---|---|---|---|---|---|---|---|---|
| TY-034 | 0.67 | 0.82 | 8.76 | 50.09 | 2.11 | 7.41 | 0.38 | 6.89 | 103.28 | 4.81 | 12.53 |
| TY-033 | 0.58 | 3.52 | 6.25 | 47.40 | 1.53 | 15.05 | 0.24 | 2.93 | 53.65 | 42.92 | 9.58 |
| TY-032 | 0.32 | 0.85 | 1.35 | 14.12 | 0.31 | 45.84 | 0.06 | 1.15 | 289.98 | 36.42 | 12.41 |
| TY-031 | 0.37 | 1.57 | 6.16 | 49.19 | 1.49 | 12.34 | 0.38 | 6.07 | 191.60 | 11.37 | 14.33 |
| TY-030 | 0.39 | 1.21 | 7.50 | 50.81 | 1.79 | 13.96 | 0.60 | 5.20 | 73.02 | 10.97 | 8.61 |
| TY-029 | 0.49 | 0.83 | 9.70 | 46.99 | 2.27 | 7.73 | 0.83 | 8.71 | 84.89 | 7.26 | 10.87 |
| TY-028 | 0.19 | 0.57 | 1.67 | 76.01 | 0.34 | 9.56 | 0.07 | 1.50 | 163.39 | 7.91 | 19.87 |
| TY-027 | 0.32 | 0.59 | 8.35 | 65.43 | 2.05 | 0.22 | 0.37 | 3.14 | 67.35 | 3.70 | 10.44 |
| TY-026 | 0.24 | 0.44 | 1.37 | 48.90 | 0.34 | 26.40 | 0.06 | 0.58 | 159.19 | 29.17 | 10.10 |
| TY-025 | 0.06 | 0.46 | 0.04 | 1.06 | 0.02 | 56.18 | 0.00 | 0.06 | 122.43 | 324.60 | 27.10 |
| TY-024 | 0.21 | 0.39 | 5.23 | 74.81 | 1.69 | 0.13 | 0.25 | 1.94 | 41.71 | 4.02 | 11.01 |
| TY-023 | 0.22 | 0.81 | 3.98 | 75.72 | 1.08 | 3.87 | 0.20 | 1.49 | 48.51 | 3.38 | 9.71 |
| TY-022 | 0.24 | 0.54 | 5.69 | 65.13 | 2.41 | 8.87 | 0.19 | 1.55 | 33.11 | 3.93 | 449.93 |
| TY-021 | 0.23 | 0.52 | 4.06 | 51.61 | 1.30 | 16.47 | 0.19 | 2.25 | 145.47 | 9.35 | 1,173.62 |
| TY-020 | 0.25 | 0.58 | 5.12 | 45.73 | 1.58 | 6.96 | 0.23 | 3.06 | 169.93 | 8.24 | 1,526.37 |
| TY-019 | 0.14 | 0.87 | 0.48 | 4.74 | 0.12 | 52.49 | 0.02 | 0.50 | 357.41 | 60.93 | 192.19 |
| TY-018 | 0.27 | 0.49 | 4.56 | 55.73 | 1.35 | 14.98 | 0.21 | 2.00 | 68.09 | 12.70 | 639.38 |
| TY-017 | 0.29 | 0.65 | 6.64 | 63.65 | 2.04 | 2.72 | 0.32 | 2.60 | 30.55 | 8.08 | 585.37 |
| TY-016 | 0.24 | 0.65 | 4.40 | 58.46 | 1.43 | 15.43 | 0.19 | 1.65 | 40.02 | 4.60 | 331.14 |
| TY-015 | 0.25 | 0.46 | 5.86 | 39.33 | 2.36 | 18.79 | 0.28 | 3.23 | 106.42 | 23.06 | 691.16 |
| TY-014 | 0.31 | 1.49 | 6.38 | 61.68 | 2.05 | 10.92 | 0.27 | 2.23 | 45.12 | 4.78 | 369.44 |
| TY-013–1 | 0.20 | 0.69 | 1.85 | 10.20 | 0.51 | 47.60 | 0.07 | 0.63 | 38.76 | 14.81 | 124.38 |
| TY-013 | 0.38 | 0.66 | 5.86 | 33.55 | 2.05 | 26.36 | 0.24 | 2.40 | 31.34 | 20.30 | 296.65 |
| TY-012 | 0.18 | 0.74 | 0.84 | 6.58 | 0.23 | 49.41 | 0.04 | 0.57 | 121.18 | 77.07 | 114.52 |
| TY-011 | 0.23 | 0.78 | 2.63 | 22.74 | 0.96 | 37.99 | 0.12 | 2.30 | 216.22 | 25.33 | 262.24 |
| TY-010 | 0.28 | 0.67 | 6.26 | 41.81 | 2.10 | 23.21 | 0.24 | 2.01 | 12.22 | 3.51 | 170.12 |
| TY-009 | 0.22 | 0.96 | 6.97 | 27.85 | 1.82 | 32.40 | 0.18 | 2.72 | 7.68 | 7.62 | 46.80 |
| TY-008 | 0.13 | 14.79 | 1.35 | 4.29 | 0.32 | 34.93 | 0.05 | 0.92 | 4.05 | 6.19 | 13.90 |
| TY-007 | 0.16 | 3.05 | 2.79 | 29.91 | 0.82 | 32.80 | 0.10 | 1.47 | 4.18 | 3.49 | 19.16 |
| TY-006 | 0.23 | 0.65 | 5.03 | 67.15 | 1.24 | 12.31 | 0.21 | 1.65 | 7.47 | 3.01 | 43.36 |
| TY-005 | 0.10 | 0.80 | 0.49 | 1.62 | 0.12 | 53.86 | 0.02 | 0.40 | 15.55 | 22.43 | 4.44 |
| TY-004 | 0.17 | 0.51 | 2.74 | 37.22 | 0.87 | 32.00 | 0.12 | 0.97 | 3.46 | 7.19 | 38.76 |
| TY-003 | 0.18 | 0.78 | 0.75 | 3.56 | 0.16 | 52.18 | 0.03 | 0.66 | 3.88 | 6.29 | 7.73 |
| TY-002 | 0.09 | 0.55 | 1.48 | 16.24 | 0.47 | 44.97 | 0.07 | 0.63 | 11.78 | 6.21 | 28.43 |
| TY-001 | 0.14 | 0.78 | 0.82 | 6.09 | 0.26 | 51.00 | 0.04 | 0.51 | 2.74 | 6.26 | 10.03 |

hydrocarbon-forming organisms and volcanic activity in the Dalong Formation will enrich the efforts in biological extinction and recovery in the Permian–Triassic boundary (PTB) and then help to strengthen the understanding of the Earth's ecological environment in this major transition of geological history.

## 2 GEOLOGICAL SETTING

In the Upper Permian, the Sichuan Basin was a marine craton basin (Li et al., 2015), with mainly carbonate rocks deposited. According to the fossil community and habitat types in Shangsi, Guangyuan, classified by Yan et al. (2008), and the habitat type classification of Yin and Tong (1995), the Dalong Formation indicates lower shallow sedimentary environment in the lower and upper parts and intra-platform basin sedimentary environment in the middle part.

This thesis takes the Shangsi Dalong Formation in Guangyuan, Sichuan Province, as the research object (**Figure 1**). Dalong Formation is mainly distributed as two strips in northwestern and northern Sichuan Basin. The study area is located in the Kuangshanliang-Liangping area, Guangyuan, in a narrow coverage striking NW-SE, where the strata are about 10–40 m thick and gradually thin to the southwest and northeast (Fu et al., 2010) (**Table 1**).

Except for the Dalong Formation, the Xuanwei Formation is mainly developed in the Upper Permian in the Emei-Junlian area, western Sichuan Basin, and it is composed of argillaceous sandstone and shale, as well as coal seams, with rich Gigantopterisian flora (Yang, 2016). The bottom of the Xuanwei Formation is tuff or conglomerate, which is in disconformable contact with the Emeishan basalt. Approaching the top, the coal seam gradually disappears until the overlying Kayitou Formation and Dongchuan Formation. In central Sichuan Basin, the Upper Permian strata are Longtan Formation and Changxing Formation from the bottom to the top. The Longtan Formation is believed to be transitional sedimentary facies, mainly depositing black silty mud shale, with a few limestone and occasionally intercalated with coal streaks, and it is in parallel unconformable contact with the underlying Maokou Formation (Yang et al., 2021). The Changxing Formation is of marine platform sedimentary facies, represented by marl and sandy mudstone, and it has

rich biological fossils, including foraminifera, brachiopods, and bivalves (Zhang and Zhang, 1992; Ma et al., 2006; Ran et al., 2021). The Changxing Formation and the overlying Feixianguan Formation are bounded by thin mudstone and marl (**Figure 2**).

# 3 SAMPLES AND METHOD

The outcrop section in Xibei Township of Guangyuan includes the Permian and Triassic strata. The top of Permian Changxing Formation, the whole Dalong Formation, and the bottom of Triassic Feixianguan Formation were measured, with the thickness of 30.80 m. The Permian Changxing Formation at the bottom of the section is about 2.50 m thick and contains mainly gray limestone with chert strip (**Figure 3A**). Upward, the Dalong Formation appears, with a total thickness of about 27.80 m, and mainly contains black mudstone and shale, with a high silicon content. There is an argillaceous limestone section of about 1.00 m at the bottom of the Dalong Formation (**Figure 3B**). Silicon content increases toward the middle of the Dalong Formation. There are massive black shale and black siliceous mud shale with limestone lens in the middle (**Figure 3C**), and two thin layers of limestone are found. The top of the Dalong Formation is gray limestone of about 4.00 m. Triassic stratum is deposited at the top of the section, with a thickness of about 0.50 m, and containing mainly gray marl. **Figure 3D** shows a part of volcanic ash samples collected.

A total of 113 samples were acquired from the field outcrop, including 98 shale samples and 15 volcanic ash (tuff) samples. The shale samples were numbered as TY-001 to TY-091 in a descending order of age (**Figure 4**), the thickness of volcanic ash layer is between 1 and 5 cm, and it is concentrated in 1–3 cm. They were analyzed for TOC and XRF measurement, kerogen pyrolysis, rock slice, and maceral observation. The pyrolysis test was conducted in China University of Petroleum (Beijing), and the XRF and ICP-MS tests were conducted in China University of Geosciences (Wuhan). Specifically, the XRF test was completed using PANalytical Zetium and the Super Q 6 analysis software, with the sample preparation steps as follows: 1) pre-oxidation and melting; and 2) determination of loss on ignition. The ICP-MS and pyrolysis tests were completed according to the procedures described by Govindaraju (1994) and Song et al. (2012).

# 4 RESULTS

## 4.1 Organic Matter Content, Total Sulfur, and Rock Pyrolysis

The Longfeng quarry section is found with obvious cyclicity of lithology, roughly as a succession (from the bottom to the top) of limestone–mud shale–limestone–mud shale–mud shale interbedded with limestone lens–limestone (**Figure 4**). The silicon content is generally high. TOC varies obviously with lithology, and exhibits relatively higher value in black shale.

The analysis results show that the TOC value is universally high in the section, ranging from 0.1% to 15.5%, with an average of 4.8% (5.2% in the Dalong Formation). The highest TOC value (15.5%) is demonstrated in the middle part of the Dalong Formation. The total sulfur content (TS) is 1.2% on average, but it changes greatly in the vertical direction. In other words, the appearance of volcanic ash layer rapidly increases the TS. The minimum and maximum of TS in the Dalong Formation are 0.1% and 4.7%, respectively, and reveal the largest difference of 3.6% between two neighbor samples, typically near the N11 volcanic ash layer.

The results of rock pyrolysis show that the hydrocarbon-generating potential (S1 + S2) of the Dalong Formation is 0.04–19.76 mg/g, with an average of 5.78 mg/g, the peak temperature (Tmax) of thermolysis changes little in the Dalong Formation, with an average of about 446°C, and S1/(S1 + S2) ranges between 0.1 and 0.2, indicating that the Dalong Formation stays at the peak or late stage of hydrocarbon generation, with a high maturity of organic matters. The HI value ranges from 33.86 to 1,139.47, primarily in 80–120, with an average of 108.13, and it increases obviously in the rocks below to above the volcanic ash layers—even from 44.04 to 587.83, especially near the N20 volcanic ash layer (**Figure 5**).

## 4.2 Inorganic Elements

For major elements, $SiO_2$, $Al_2O_3$, and $Fe_2O_3$ account for relatively high proportions, being about 55.13%, 4.47%, and 2.10%, respectively; the proportions of $K_2O$, MgO, $Na_2O$, and $TiO_2$ are relatively low, accounting for 1.02%, 1.21%, 0.33%, and 0.17%, respectively. Moreover, the CaO content is high, with an average of about 15.43%, and it is higher in the upper and lower parts than in the middle part of the Dalong Formation. For trace elements, MOEF, UEF, and VEF are 148.72, 16.71, and 226.75 on average, respectively, with higher enrichment coefficient, and all values are higher in the layers above the volcanic ash layer than those beneath the volcanic ash layer.

# 5 DISCUSSION

## 5.1 Geochemical Characteristics of Source Rocks in Dalong Formation

Under normal thermal evolution conditions, the abundance of organic matter in rock is directly proportional to the hydrocarbon-generating capacity (Mukhopadhyay et al., 1985), and the conventional indicators for evaluating the abundance of organic matter include TOC, chloroform asphalt "A," hydrocarbon-generating potential (S1 + S2), and total hydrocarbon (Liu et al., 2008; Liu et al., 2016). However, in the case of high-evolution degree, TOC becomes the main indicator to evaluate the hydrocarbon-generating potential of source rocks (Fu et al., 2010).

In this thesis, TOC was mainly used to evaluate the hydrocarbon-generating potential of the Dalong Formation, which has a high thermal evolution degree (Fu et al., 2010). As shown in **Figures 4** and **5**, the appearance of volcanic ash layer affects TOC, TS, pyrolytic hydrocarbon (S2), and HI of the Dalong Formation. For samples from the strata above the volcanic ash layer, both TOC and TS increase to a certain extent. For samples adjacent to volcanic ash above the

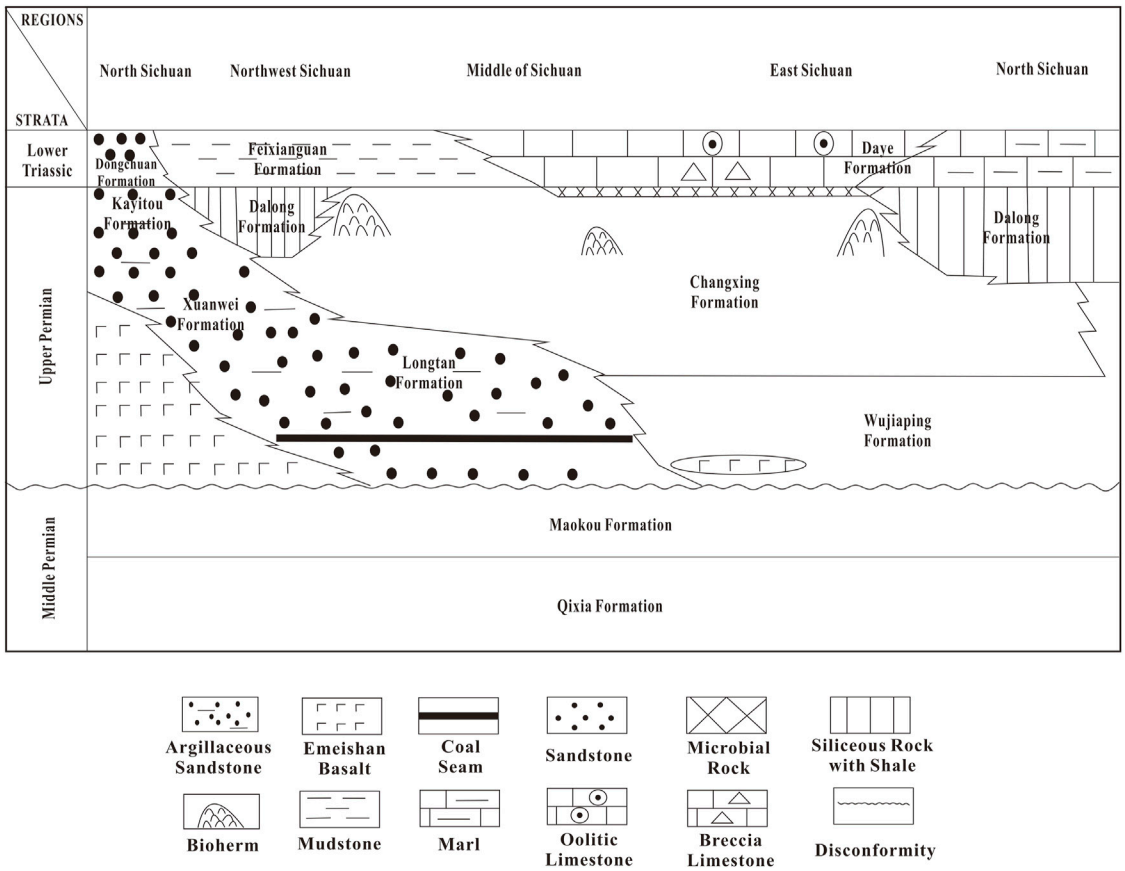


**FIGURE 2 |** Stratigraphic division of Sichuan Basin (modified after Yang, 2016).

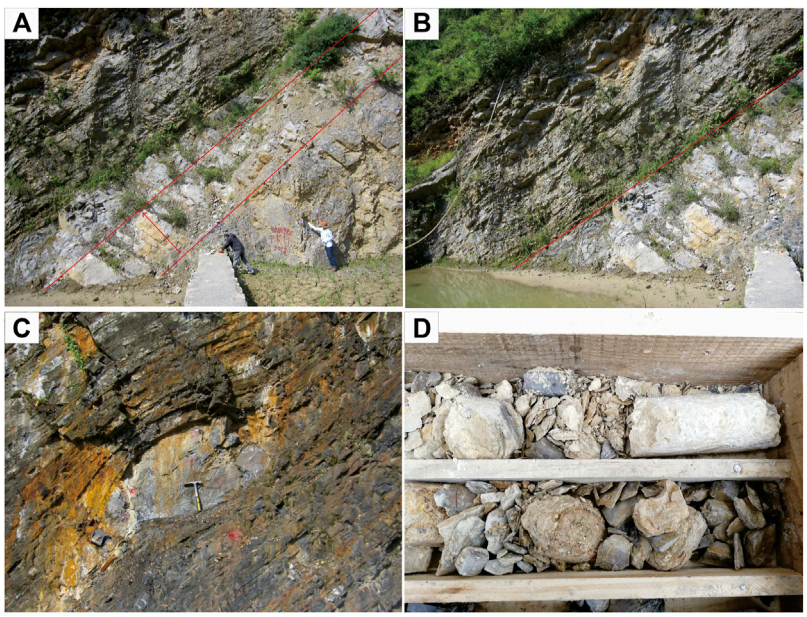


**FIGURE 3 |** Longfeng quarry section near Shangsi, Guangyuan.

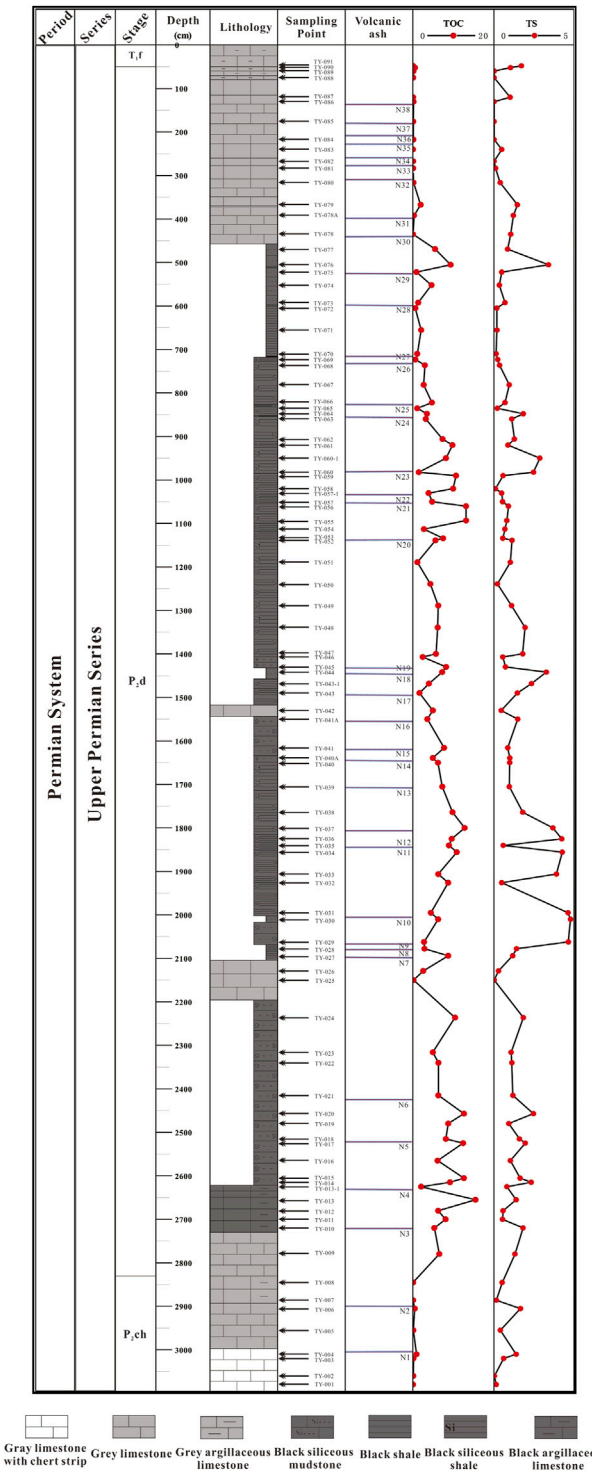


**FIGURE 4 |** Longfeng quarry profile sampling location and sample TOC and TS data.

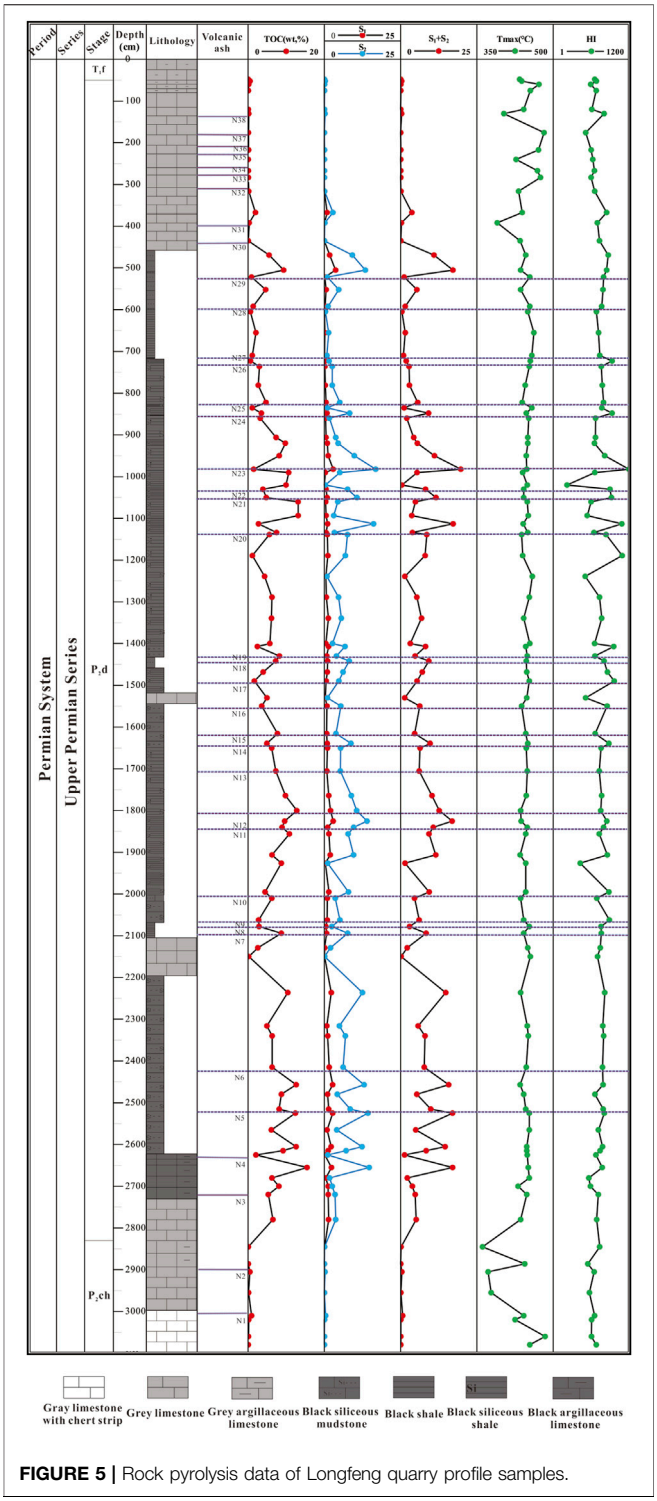


**FIGURE 5 |** Rock pyrolysis data of Longfeng quarry profile samples.

volcanic ash layer, TOC increases slightly, but S2 and HI increase rapidly. This phenomenon, different from the common viewpoint that TOC should change in the same trend as S2, may be attributed to the fact that the huge input of insoluble substances by volcanic eruption into water greatly diluted TOC, while the facilitation of volcanic ash to the growth of hydrocarbon-forming organisms (at this time, the hydrocarbon-generating potential was increasing) resulted in the increase of S2. Moreover, a higher HI represents a higher

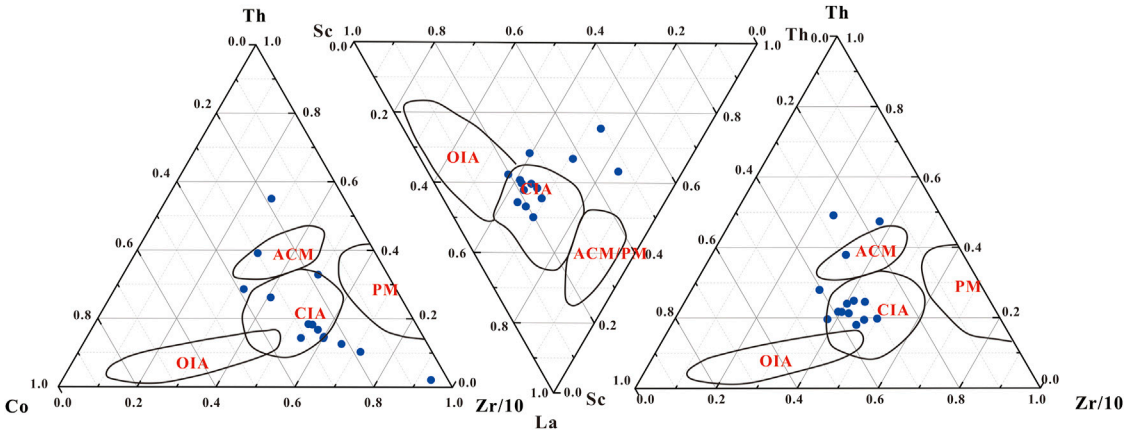


**FIGURE 6 |** Tectonic setting of Permian Dalong Formation in Longfeng quarry section. (Bhatia, 1984; Roser and Korsch, 1988). OIA, ocean island arc; CIA, continental island arc; ACM, active continental margin; PM, passive margin.

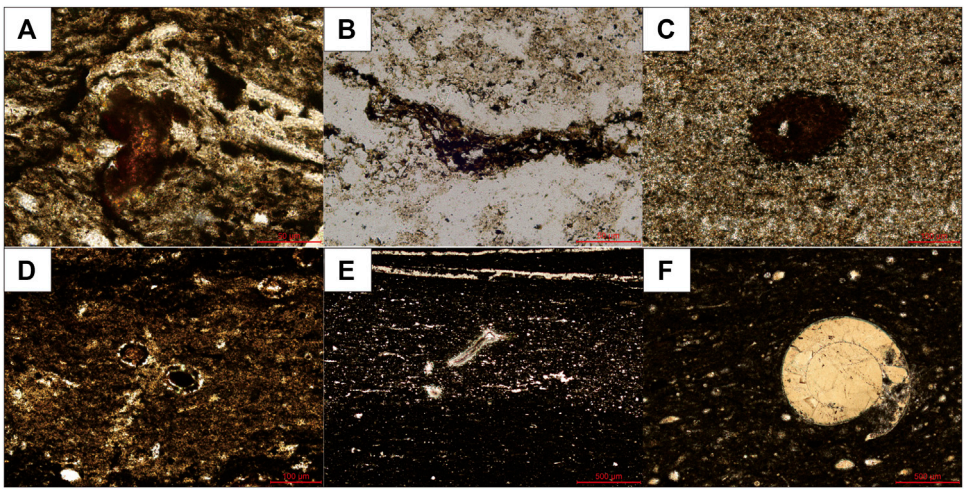


**FIGURE 7 |** Biological fossils of Dalong Formation in Longfeng quarry section. **(A)** Planktonic algae; **(B)** benthic algae; **(C)** acritarchs; **(D)** radiolaria; **(E)** sponge spicule; and **(F)** foraminifera.

hydrocarbon-generating capacity. For example, bacteria and algae show high HI value due to their high lipid contents, and the change in types of hydrocarbon-forming organisms/organic matters can be expressed by HI (Peters et al., 2005). The samples above the volcanic ash layer reflect apparently increasing HI, indicating that the association of hydrocarbon-forming organisms and the proportions of organisms changed, with planktonic algae taking a higher share in hydrocarbon-forming organisms (Meng et al., 2022).

## 5.2 Tectonic Setting of Source Rocks in Dalong Formation

Previous studies have shown that some trace elements (e.g., Th, V, Co., and Zr) have stable properties and are not easy to migrate. The triangular diagrams of Th–Co–Zr/10, La–Th–Sc, and Th–Sc–Zr/10 can be used to distinguish the tectonic setting of the provenance (Ross and Bustin, 2009).

It can be seen from **Figure 6** that the samples of the Dalong Formation are mainly distributed in ACM and CIA. The data processing results correspond to the frequent plate activity during the deposition of the Late Permian Dalong Formation in the Sichuan Basin, and they are consistent with the characteristics of frequent volcanic activity and multi-stage distribution of volcanic ash in the study area. Comprehensive analysis indicates that the element mass fraction of the Dalong Formation is closer to the characteristic values of ACM and CIA. It is thus determined that the Dalong Formation was deposited under a tectonic setting of ACM and CIA. This conclusion is consistent with the research results of Liu et al. (2019) on the Dalong Formation in western Hubei Province, which is covered in the same tectonic range as Shangsi of Guangyuan, both in the central-north of the Yangtze plate.

## 5.3 Regular Vertical Distribution of Hydrocarbon-Forming Organisms in Dalong Formation

Abundant fossils of biota (including plankton and benthos) and other organisms (including sponge spicule, ammonite, and brachiopod) are identified in the Dalong Formation of the Longfeng quarry section.

Combined with previous studies and the thin section identification of organic petrology in this study, it is found that the hydrocarbon-forming organisms of the Dalong Formation are mainly planktonic and benthic. The thin sections reveal the thalluses of planktonic algae (**Figure 7A**) and benthic algae (**Figure 7B**), as well as biological fossils, such as acritarchs that are suspected to be derived from planktonic algae (**Figure 7C**), radiolarians (**Figure 7D**), sponge spicules (**Figure 7E**), and planktonic foraminifera (**Figure 7F**).

The Dalong Formation in Shangsi, as a whole, was deposited in shallow sea and shelf facies sedimentary environment (Hu G. et al, 2021). Most of the fauna lived in the lower part of shallow sea, and the association and distribution of organisms show that the Dalong Formation was always in a reducing and low-energy environment during its deposition.

The hydrocarbon-forming organisms in Dalong Formation vary obviously in vertical direction. In the lower part near the Changxing Formation, there are few volcanic ash layers, which acted at large time intervals, giving rise to organisms with low content and single types (dominantly minor radiolarians and some algal fragments). In the middle part, due to frequent volcanic activity, multiple volcanic ash layers with smaller spacing appeared, and the organism association is dominated by radiolarians, calcium spheres, and algal debris, of which radiolarians take a very high proportion in the biological community because siliceous organisms could grow without competitors, especially in the water area with sufficient clay supply (Cai et al., 2011). In the upper part, there are also numerous volcanic ash layers, and organisms are abundant in quantity and species, which are mainly foraminifera, gastropods, conodonts, calcium spheres, and radiolarians, as well as association of other biological fossils; the proportion of radiolarians is high, but far less than that in the middle part (**Figure 8**).

## 5.4 Volcanic Activity-Related Development of Hydrocarbon-Forming Organisms in Dalong Formation

A total of 98 shale samples were taken from 30.80 m thick strata in the Longfeng quarry section, and revealed 38 layers of volcanic ash and tuff, including 36 layers in the Dalong Formation. Considering the higher accuracy of sampling than thin section observation, typical samples above and below the representative N17–N19 and N22 volcanic ash (tuff) layers were selected for depiction. These layers were chosen because of the following reasons: 1) TOC and TS increase significantly after the deposition of these layers; 2) TOC and TS increase step-like continuously due to the N17–N19 volcanic ash layers which are adjacent with each other and thus can be analyzed to verify whether the influence of volcanic ash layers can be stacked; and 3) TOC curve shows a trend of sharp increase–slow increase–sharp

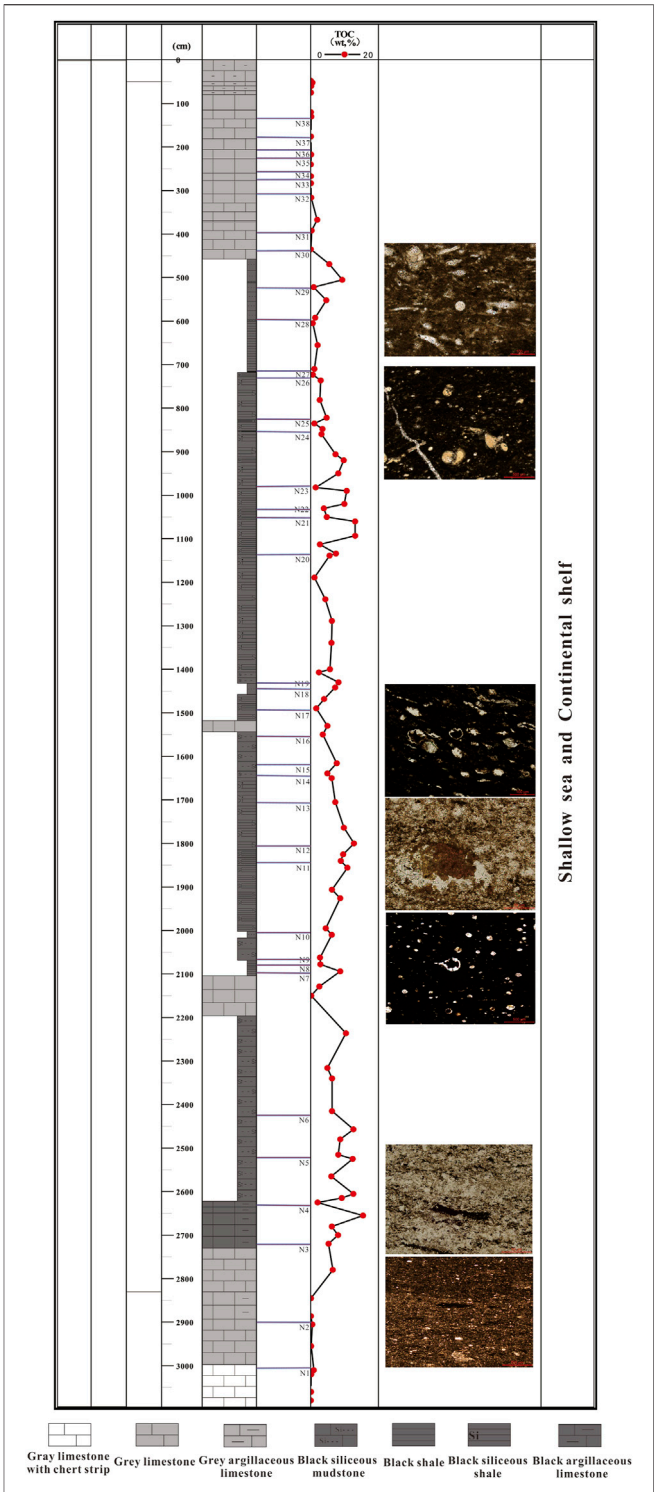


**FIGURE 8 |** Vertical variation of organism types in Dalong Formation in Longfeng quarry section.

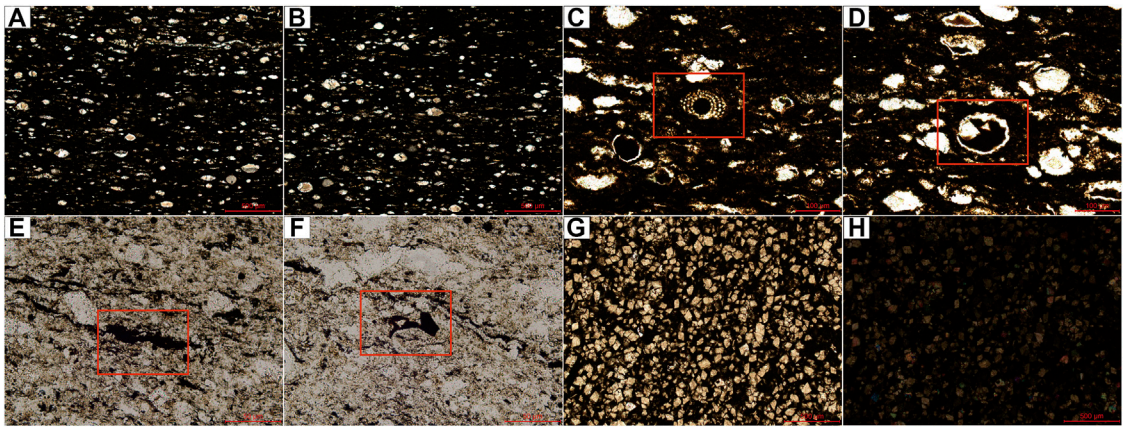


**FIGURE 9 |** Hydrocarbon-forming organisms above and below N17–N19 volcanic ash layers. **(A,B)** Radiolaria, above N19; **(C)** foraminifera, above N18; **(D)** radiolaria, above N18; **(E)** algal debris, above N17; **(F)** biological nail plate, above N17; **(G,H)** stellate organic matter, below N17.

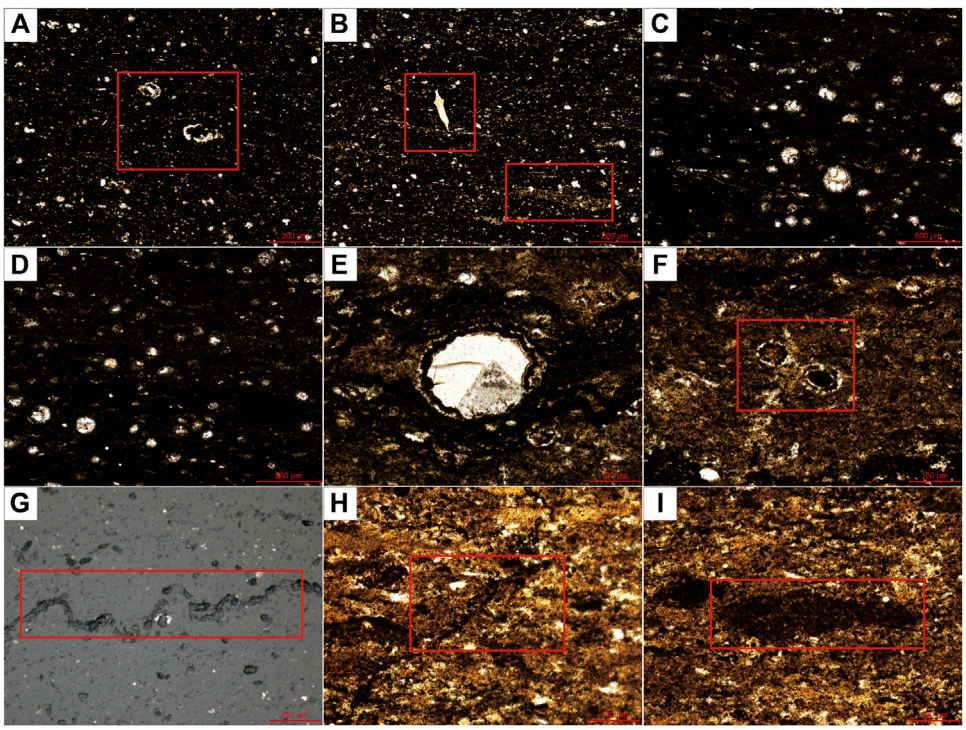


**FIGURE 10 |** Hydrocarbon-forming organisms above and below N22 volcanic ash layer. **(A,B)** Biological nail plate and algal debris, above N22 and close to N23; **(C–F)**: radiolaria, above N22; **(G)** worm trail, below N22; **(H,I)** benthic algal thallus, below N22.

decrease, under the control of the N22 volcanic ash layer, which can be analyzed to find out the reason why this TOC trend occurs.

### 5.4.1 Different Hydrocarbon-Forming Organisms Below and Above Volcanic Ash Layers

The N17, N18, and N19 volcanic ash (tuff) layers are densely distributed, with TOC increasing in a step-like manner, which may be due to the stacked effect of volcanic ash. Below N17, TOC is 1.65%; above N17, TOC increases to 3.96%, nearly doubled. After N18, TOC increases again to 7.25%. After N19, TOC increases slightly again, from 7.25% to 8.22%. Below and above N17 and N18, there are obvious changes in the number and type of hydrocarbon-forming organisms. Below N17, TOC is low, thin sections are rarely observed with traces of biological fossils and biological activities, and organic matters are dispersed and stellate embedded in the mineral matrix (**Figures 9A,B**).

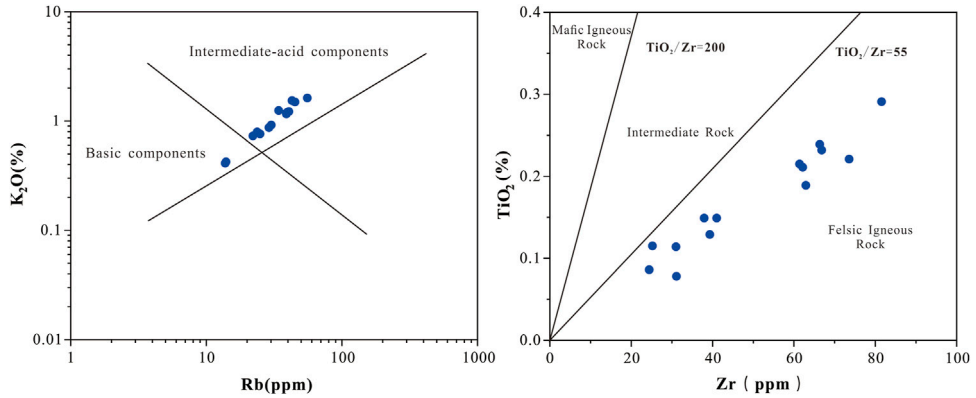


**FIGURE 11 |** $K_2O$–Rb and $TiO_2$–Zr diagram of Longfeng quarry section.

**TABLE 2 |** Components of magma by types.

| Magma type | $SiO_2$ content | Features of other components |
|---|---|---|
| Ultrabasic magma | <45% | Rich Fe and Mg, low Ca, and poor K and Na |
| Basic magma | 45%–53% | High Fe, Mg, and Ca and low K and Na |
| Intermediate magma | 53%–66% | Moderate Fe, Mg, Ca, Na, and K |
| Acidic magma | >66% | Low Fe, Mg, and Ca and high K and Na |

Above N17, obvious biological fossils are observed, mainly broken biological nail plates of suspected benthic organisms (**Figure 9C**) and fragments of benthic algae and thallus (**Figure 9D**). Near the top of the Dalong Formation, the major observed organisms are foraminifera and radiolarians (**Figures 9E,F**). After N18, the concentration of nutrient elements further increases and the number of hydrocarbon-forming organisms increases sharply; thin sections show a large number of radiolarians with great density and many biological trace fossils such as calcium spheres and algal debris (**Figures 9G,H**).

After N22, TOC also changes significantly—from 3.90% to 9.95%, nearly tripled. It is noteworthy that such sharp increase of TOC lasted only for a short period, followed by a slow increase to 10.65% and finally a sharp decrease to 1.48%. With the thin section observation, this TOC variation is speculated to occur in the process as follows: the content of nutrient elements in water surged in a short time after the partial dissolution of volcanic ash, which brought quickly a large number of nutrient elements to planktons and benthos, making them grow rapidly in quantity; when the biological density approached the level the water could bear, the growth of these hydrocarbon-forming organisms slowed down apparently; after the biological density reached the extreme level the environment could carry, the organisms no longer increased, and massive organisms died as a result of huge oxygen consumption in biological respiration.

The aforementioned speculation was verified by thin section observations of samples from rocks above and below N22. A small quantity of scattered fragments of planktonic algae, foraminifera, radiolarians, and traces of biological activities were observed in the stratum below N22 (**Figures 10A–C**). In the stratum above N22, there are much more hydrocarbon-forming organisms, which are mainly radiolarians, and also abundant siliceous radiolarian shells (**Figures 10D,G**), which is also one of the reasons for the extremely developed siliceous rocks in the Dalong Formation of Longfeng quarry section. After a period since the deposition of N22, TOC decreased rapidly, and only sporadic biological nail plates and traces of algae (e.g., algal debris and leaf residues) were developed (**Figures 10H,I**), as evidenced by the corresponding thin sections.

### 5.4.2 Factors Affecting the Development of Hydrocarbon-Forming Organisms

There is sufficient evidence to justify the positive impact of volcanic ash on the development of hydrocarbon-forming organisms. For example, the eruption of Kasatochi volcano in 2008 prompted the algae bloom in an area of (1.5–2.0) × 106 $km^2$ in northeastern Pacific Ocean (Langmann, 2013). However, it is still not clear why and how the hydrocarbon-forming organisms were affected by volcanic ash. Here, the possible factors are preliminarily discussed from the perspective of element geochemistry.

#### *5.4.2.1 Magmatic Properties*

Generally, the Emeishan large igneous province is mainly composed of subalkaline and meta-alkaline basic volcanic lavas and pyroclastic rocks (Mei, 1973; Meng et al., 2018). However, acidic volcanic rocks were also exposed in the late stage of

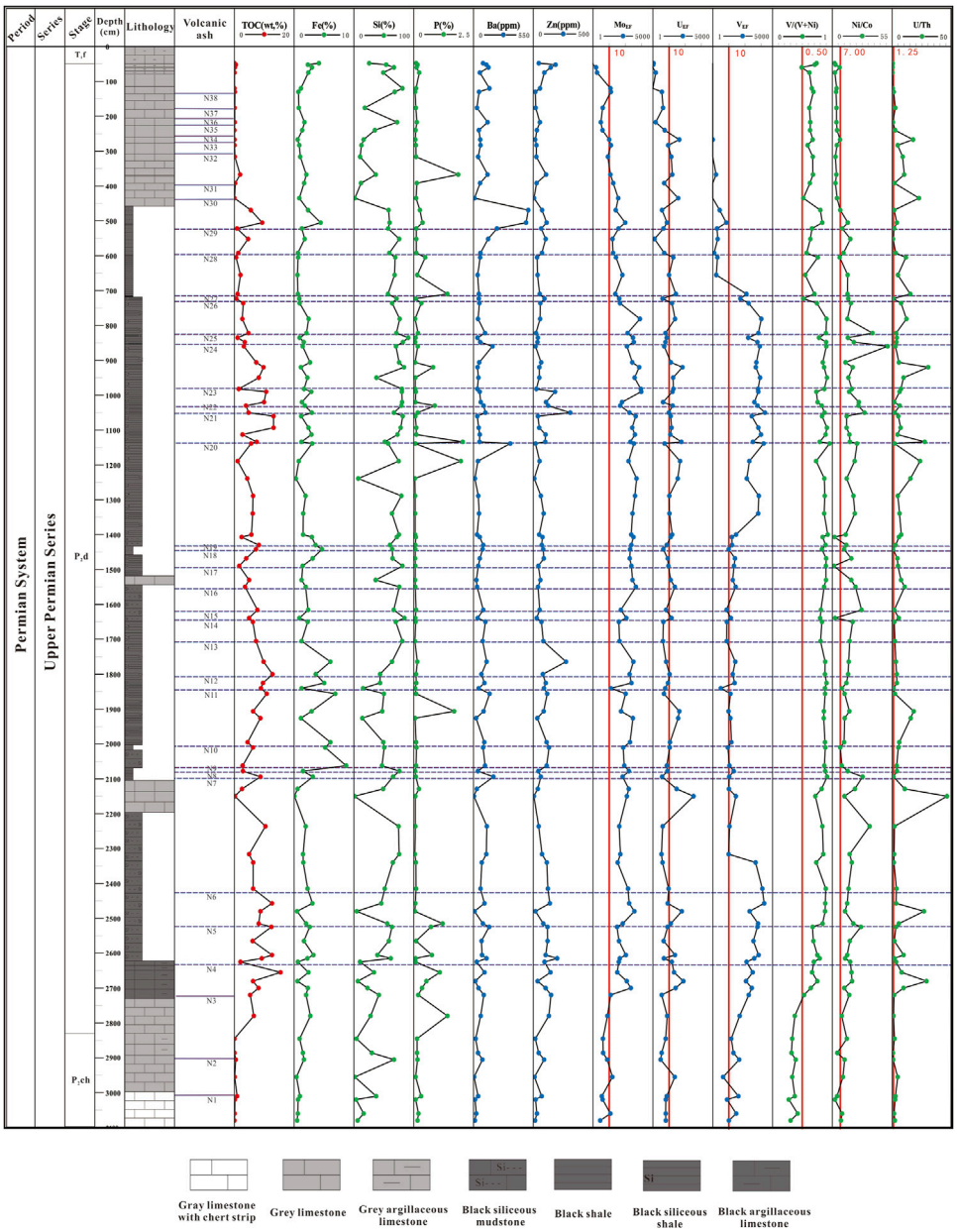


**FIGURE 12 |** Geochemical element indexes of Longfeng quarry profile.

magmatism. They coexist with basic volcanic rocks and show the bimodal features (Xu et al., 2010).

Acidic volcanic rocks are mainly trachyte and rhyolite. They are somewhat different from basic basalt in composition. Trachyte contains significantly less MgO, Fe2O3, P2O5, TiO2, and CaO and reflects obvious Eu negative anomaly and strong loss of Sr, Ti, and other elements (Xu et al., 2013). Different types of magma are distinct in components (Hu et al., 2019).

Based on the chart of Taylor et al. (1985), the $K_2O$–Rb and $Zr–TiO_2$ diagrams were obtained from the data of Longfeng quarry section (**Figure 11**). It can be seen that $K_2O$ accounts for 0.1%–8.0%, and Rb is concentrated at 10–100 ppm, it shows that the three symbolic volcanic ash layers mentioned above are intermediate-acid components. According to the $Zr–TiO_2$ diagram, the three marked volcanic ash layer combinations of Dalong formation are dominated by felsic igneous rocks, which also indicate acidic magma. Combined with the compound composition of the Dalong Formation and the components of magma in **Table 2**, it can be basically determined that the volcanic ash affecting the development of hydrocarbon-forming organisms in the Longfeng quarry section is mainly acidic magma.

It is found that the magma of N17–N19 and N22 all fall in the region of intermediate-acid components. The intermediate-acid

magma can play a better role in promoting the development of hydrocarbon-forming organisms, possibly because they could provide sufficient and comprehensive nutritional elements, including Si, Fe, Mg, Ca, Na, and K, of which Fe is decisive for biological growth.

#### *5.4.2.2* Different Element Inputs

The deposition of N22, TOC, Si, Zn, and Mo increased (**Figure 12**), which proves that volcanic ash can indeed cause the increase of element concentration in a certain period and promote the growth of hydrocarbon-forming organisms. However, Fe and P decreased to some extent, which is not attributable to the probability that the volcanic ash did not carry these elements, but more likely that these elements were consumed faster than that before volcanic ash deposition. Particularly, the decrease of P lasted for a long time, while the decrease of Fe only lasted for a short time, possibly because Fe was not the controlling element at this time, but the large input of Zn promoted the utilization of phosphate by algae, resulting in the reduction of P. Referring to **Figure 10**, after the deposition of N22, more traces of benthic algae, planktonic algae, and radiolarian were found in the stratum. After the deposition of N17, TOC, Fe, Cu, Zn, and Mo all increased greatly, P was always at a low level, and Si decreased significantly, indicating that P was the most likely element restricting the growth of organisms at this time, and the input of Si enriched the nutrients for hydrocarbon-forming organisms (Meng et al., 2009). Referring to **Figure 8**, after volcanic ash deposition, the number of radiolarians and foraminifera of benthic and planktonic species increased owing to the input of Si, Mo, Fe, and other elements.

#### *5.4.2.3 Time Interval of Volcanic Activities*

Observation of spacing between volcanic ash layers indicates that during the deposition of N30–N38 volcanic ash layers, the curves of TOC and elements show minor variation. However, this phenomenon rarely occurs in other layers, and it is presumably caused by the too short time interval of volcanic activities. On the one hand, the deposition of multiple volcanic ash layers in a short time would cause the incomplete release of nutrients, and exert an inconspicuous effect in promoting the growth of hydrocarbon-forming organisms. On the other hand, multiple volcanic activities in a short time might induce a higher concentration of toxic substances inhibiting the growth of hydrocarbon-forming organisms in water. The microscopic identification results of hydrocarbon-forming organisms shown in **Figure 10** also suggest that algae is very rare in the thin-section view of samples from above N22 with frequent volcanic activities (**Figures 10A–H**), while algae can be seen in samples from below N22 (**Figures 10G–I**). Nonetheless, further efforts are needed to determine which action ultimately led to the TOC reduction in layers with dense volcanic ash.

## 6 CONCLUSION

(1) The samples of the Dalong Formation taken from the Longfeng quarry section in Shangsi of Guangyuan, Sichuan Basin, were analyzed in light of major trace elements, the enrichment coefficients of paleo-productivity indicator elements (N, P, and Fe etc.) and redox indicator elements (Mo, U, and V), and V/(V + Ni), Ni/Co, and U/Th. It is found that volcanic activity contributed to the increase of TOC and made the sedimentary environment highly reducing.

(2) The hydrocarbon-generating materials of the Dalong Formation include benthic algae, planktonic algae, acritarchs, radiolarians, and foraminifera, of which radiolarians take a high proportion. Vertically, at the bottom of the Dalong Formation, hydrocarbon-forming organisms are small in quantity and single in types; in the middle part, hydrocarbon-forming organisms are dominated by plankton and benthos, with radiolarians as the biological fossil with the largest proportion; in the middle–upper part, hydrocarbon-forming organisms are mainly plankton and acritarchs, with abundant foraminifera and broken nail plates of various organisms.

(3) According to the analysis of the components of magma formed by volcanic eruptions in different periods during the deposition of the Dalong Formation, the magma type has an impact on the development of hydrocarbon-forming organisms. It is preliminarily determined that the intermediate (intermediate-acid) magma has a better effect on promoting the development of hydrocarbon-forming organisms. In addition to magmatic properties, different element inputs and time intervals of volcanic activities may have significant impact on the number and types of hydrocarbon-forming organisms. Specifically, different element inputs would induce the development of different aquatic plankton and benthos. Too small time interval of volcanic activities might make the nutrient elements of volcanic ash fail to release completely, or the accumulation of elements inhibiting the development of hydrocarbon-forming organisms brought by volcanic ash might result in the worse growth of hydrocarbon-forming organisms.

## DATA AVAILABILITY STATEMENT

The original contributions presented in the study are included in the article/supplementary material; further inquiries can be directed to the corresponding authors.

## AUTHOR CONTRIBUTIONS

CZ carried out the experiment and wrote the manuscript. QM designed the whole research, set up the tech geological model, and modified the manuscript. ZS analyzed other paleontology other than algae, such as foraminifera. XT analyzed the source rock type and the favorable factors for organic matter enrichment. QP analyzed the characteristics of algae. DL analyzed the sedimentary environment, and DZ and JYL jointly processed the primary color characteristics of the rock. JCL collected samples and performed pretreatment. BJ systematically processed the elemental analysis data.

## FUNDING

This work is jointly funded by the National Key R&D Program (2019YFA0708504), the National Natural Science Foundation Project (41872164), and the Open Fund of the State Key Laboratory of Organic Geochemistry (SKLOG202125).

## ACKNOWLEDGMENTS

This work was completed with the help of Professor Hu Guang of Southwest Petroleum University in treatment and identification of hydrocarbon-forming organisms and the assistance of Yu Xin of Peking University in field outcrop measurement.

## REFERENCES

Bhatia, M. R. (1984). Composition and Classification of Paleozoic Flysch Mudrocks of Eastern Australia: Implications in Provenance and Tectonic Setting Interpretation. *Sediment. Geol.* 41, 249–268. doi:10.1016/0037-0738(84)90065-4

Cai, X. F., Feng, Q. L., Gu, S. Z., and Luo, Z. J. (2011). Regressive Shelf Facies: an Important Part of the Formation of Source Rocks—Taking the Dalong Formation of the Upper Permian on the Northern Margin of the Middle and Upper Yangtze Region as an Example. *Oil gas Geol.* 32, 29–37.

Du, J. X., Shi, W. W., Zhou, H., Wang, Q. L., Xia, Q. J., et al. (2014). Zircon Chronology and Formation Model of Volcanic Rocks in Nanpu Sag, Bohai Bay Basin. *Oil Gas Geol.* 35, 742–748.

Duggen, S., Croot, P., Schacht, U., Hoffmann, L., and Hoffmann, L. (2000). Subduction Zone Volcanic Ash Can Fertilize the Surface Ocean and Stimulate Phytoplankton Growth: Evidence from Biogeochemical Experiments and Satellite Data. *Geophys. Res. Lett.* 34, 1–5. doi:10.1029/2006GL027522

Duggen, S., Croot, P., Schacht, U., and Hoffmann, L. (2007). Subduction Zone Volcanic Ash Can Fertilize the Surface Ocean and Stimulate Phytoplankton Growth: Evidence from Biogeochemical Experiments and Satellite Data. *Geophys. Res. Lett.* 34, 5–1612. doi:10.1029/2006GL027522

Fu, X. D., Qin, J. Z., Teng, G. E., and Wang, X. F. (2010). Evaluation of Source Rocks of Dalong Formation of Upper Permian in the Northern Margin of Sichuan Basin. *Pet. Exp. Geol.* 32, 566–571.

Gao, Y., Wang, P., Cheng, R., Wang, G., Wan, X., Wu, H., et al. (2009). Description of Cretaceous Sedimentary Sequence of the First Member of the Qingshankou Formation Recovered by CCSD-SK-Is Borehole in Songliao Basin: Lithostratigraphy, Sedimentary Facies, and Cyclic Stratigraphy. *Earth Sci. Front.* 16, 314–323. doi:10.1016/s1872-5791(08)60081-0

Govindaraju, K. (1994). 1994 Compilation of Working Values and Sample Description for 383 Geostandards. *Geostand. Newslett* 18, 1–158. doi:10.1046/j.1365-2494.1998.53202081.x-i1

Hu, D., Wang, L., Zhang, H., Duan, J., Xia, W., Liu, Z., et al. (2021a). Discovery of Carbonate Source Rock Gas Reservoir and its Petroleum Geological Implications: A Case Study of the Gas Reservoir in the First Member of Middle Permian Maokou Formation in the Fuling Area, Sichuan Basin. *Nat. Gas. Ind. B* 8 (1), 13–23. doi:10.1016/j.ngib.2020.07.001

Hu, G., He, F., Mi, J., Yuan, Y., and Guo, J. (2021b). The Geochemical Characteristics, Distribution of Marine Source Rocks and Gas Exploration Potential in the Northwestern Sichuan Basin, China. *J. Nat. Gas Geoscience* 6 (4), 199–213. doi:10.1016/j.jnggs.2021.07.004

Hu, Z. Y., Fu, W., Luo, P., Cai, Q., and Feng, M. (2019). Symbiotic Enrichment Characteristics and Genesis of Ilmenite and Rare Earth in Igneous Weathering Crust in Southeast Guangxi. *Rare earth* 40, 16–27.

Langmann, B. (2013). Volcanic Ash Versus Mineral Dust: Atmospheric Processing and Environmental and Climate Impacts. *Isrn Atmos. Sci.* 2013, 1–17. doi:10.1155/2013/245076

Lee, C.-T. A., Jiang, H., Ronay, E., Minisini, D., Stiles, J., and Neal, M. (2018). Volcanic Ash as a Driver of Enhanced Organic Carbon Burial in the Cretaceous. *Sci. Rep.* 8. doi:10.1038/s41598-018-22576-3

Li, G. Y. (2010). *Formation Conditions and Main Controlling Factors of Upper Carboniferous Volcanic Rock Reservoir in Malang Sag*. Santanghu Basin. Beijing: China University of Geosciences (Beijing) Press.

Li, J., Yang, S., Qi, Z., Zhao, G., Yin, B., and Mo, F. (2020). A Calculation Model for Water Breakthrough Time of Gas Wells in Gas Reservoirs with Edge Water Considering Interlayer Heterogeneity: A Case Study of the Lower Triassic Feixianguan Gas Reservoirs in the Puguang Gas Field. *Nat. Gas. Ind. B* 7 (6), 631–638. doi:10.1016/j.ngib.2020.04.005

Li, W., Liu, J. J., Deng, S. H., Zhang, B. M., and Zhou, H. (2015). Nature and Function of Tectonic Movement in Sichuan Basin and its Adjacent Areas from Late Sinian to Early Cambrian. *J. petroleum* 36, 546–556.

Liu, Q., Jin, Z., Liu, W., Lu, L., Meng, Q., Tao, Y., et al. (2013). Presence of Carboxylate Salts in Marine Carbonate Strata of the Ordos Basin and Their Impact on Hydrocarbon Generation Evaluation of Low TOC, High Maturity Source Rocks. *Sci. China Earth Sci.* 56, 2141–2149. doi:10.1007/s11430-013-4713-3

Liu, Q., Li, P., Jin, Z., Sun, Y., Hu, G., Zhu, D., et al. (2022). Organic-rich Formation and Hydrocarbon Enrichment of Lacustrine Shale Strata: A Case Study of Chang 7 Member. *Sci. China Earth Sci.* 65, 118–138. doi:10.1007/s11430-021-9819-y

Liu, Q., Qin, S., Li, J., Liu, W., Zhang, D., Zhou, Q., et al. (2008). Natural Gas Geochemistry and its Origins in Kuqa Depression. *Sci. China Ser. D-Earth Sci.* 51, 174–182. doi:10.1007/s11430-008-5003-3

Liu, Q., Zhu, D., Jin, Z., Liu, C., Zhang, D., and He, Z. (2016). Coupled Alteration of Hydrothermal Fluids and Thermal Sulfate Reduction (TSR) in Ancient Dolomite Reservoirs - an Example from Sinian Dengying Formation in Sichuan Basin, Southern China. *Precambrian Res.* 285, 39–57. doi:10.1016/j.precamres.2016.09.006

Liu, Q., Zhu, D., Jin, Z., Meng, Q., and Li, S. (2019b). Influence of Volcanic Activities on Redox Chemistry Changes Linked to the Enhancement of the Ancient Sinian Source Rocks in the Yangtze Craton. *Precambrian Res.* 327, 1–13. doi:10.1016/j.precamres.2019.02.017

Liu, Q., Zhu, D., Meng, Q., Liu, J., Wu, X., Zhou, B., et al. (2019a). The Scientific Connotation of Oil and Gas Formations under Deep Fluids and Organic-Inorganic Interaction. *Sci. China Earth Sci.* 62, 507–528. doi:10.1007/s11430-018-9281-2

Liu, W. Q., Qiao, Y., Bo, J. F., Mu, C. L., Tong, J. N., et al. (2019). Geochemical Characteristics of Argillaceous Rocks of Dalong Formation of Upper Permian in Enshi Area, Western Hubei and its Indication to Weathering, Provenance and Tectonic Setting. *J. Lanzhou Univ. Nat. Sci. Ed.* 55, 158–167.

Lyu, C., Zhang, Y., Li, C., Chen, G., Zhou, Q., Ma, M., et al. (2020). Pore Characterization of Upper Ordovician Wufeng Formation and Lower Silurian Longmaxi Formation Shale Gas Reservoirs, Sichuan Basin, China. *J. Nat. Gas Geoscience* 5 (6), 327–340. doi:10.1016/j.jnggs.2020.11.002

Ma, Y. S., Mou, C. L., Guo, X. S., Tan, Q. Y., and Yu, Q. (2006). Sedimentary Characteristics and Sedimentary Pattern of Changxing Period in Northeast Sichuan Basin. *Geol. Rev.*, 1, 25–29.

Mei, H. J. (1973). Relationship between Petrochemical Characteristics of Two Series of Dark Rock Abyss Differentiation in Southwest China and Iron Nickel Mineralization. *J. Geochem.*, 4, 219–253.

Meng, Q., Jing, J., Li, J., Zhu, D., Zou, A., Zheng, L., et al. (2018). New Exploration Strategy in Igneous Petroliferous Basins - Enlightenment from Simulation Experiments. *Energy Explor. Exploitation* 36, 971–985. doi:10.1177/0144598718758338

Meng, Q., Pang, Q., Hu, G., Jin, Z., Zhu, D., Liu, J., et al. (2022). Rhyolitic Ash Promoting Organic Matter Enrichment in a Shallow Carbonate Platform: A Case Study of the Maokou Formation in Eastern Sichuan Basin. *Front. Earth Sci.* 10. doi:10.3389/feart.2022.879654

Meng, Q. Q., Ma, B. L., Zou, A. D., and Li, Z. F. (2009). Comparison of Characteristics of Hydrocarbon Generation for Different Alga. *Petroleum Geol. Exp.* 30, 291.

Mukhopadhyay, P., Hagemann, H., and Jr, G. (1985). Characterization of Kerogens as Seen Under the Aspect of Maturation and Hydrocarbon Generation. *Erdol Kohle Erdgas Petrochem.* 38, 7–18.

Pang, Q. (2019). *Characteristics of Hydrocarbon-Generating Materials of Wufeng Formation and Longmaxi Formation in Changning Area and Their Influence on Organic Matter Pores*. Chengdu: Southwest Petroleum University Press.

Peters, K. E., Peters, K. E., Walters, C. C., and Moldowan, J. (2005). *The Biomarker Guide*. Cambridge, United Kingdom: Cambridge University Press.

Qiu, X. W., Liu, C. Y., Mao, G. Z., Deng, Y., and Wang, F. F. (2010). Enrichment Characteristics of Th Element in Tuff Interlayer of Yanchang Formation of Upper Triassic in Ordos Basin. *Geol. Bull.* 29, 1185–1191.

Qiu, Z., Zou, C., Wang, H., Dong, D., Lu, B., ChenLiu, Z. D. X., et al. (2020). Discussion on the Characteristics and Controlling Factors of Differential Enrichment of Shale Gas in the Wufeng-Longmaxi Formations in South China. *J. Nat. Gas Geoscience* 5 (3), 117–128. doi:10.1016/j.jnggs.2020.05.004

Ran, Q., Tao, X., Xu, C., Zhang, L., Huang, T., Liu, S., et al. (2021). Fine Description of Ramp-type Small Bioherms and Breakthrough of "two Bioherms in One Well" in High-Yield Gas Wells: A Case Study of the Changxing Formation Small Bioherm Group in the Eastern Sichuan Basin. *Nat. Gas. Ind. B* 8 (4), 384–392. doi:10.1016/j.ngib.2021.07.009

Roser, B. P., and Korsch, R. J. (1988). Provenance Signatures of Sandstone-mudstone Suites Determined Using Discriminant Function Analysis of Major-Element Data. *Chem. Geol.* 67, 119–139. doi:10.1016/0009-2541(88)90010-1

Ross, D. J. K., and Bustin, R. M. (2009). Investigating the Use of Sedimentary Geochemical Proxies for Paleoenvironment Interpretation of Thermally Mature Organic-Rich Strata: Examples from the Devonian-Mississippian Shales, Western Canadian Sedimentary Basin. *Chem. Geol.* 260, 1–19. doi:10.1016/j.chemgeo.2008.10.027

Shan, X. L., Li, J. Y., Chen, S. M., Ran, Q. C., Chen, G. B., et al. (2014). Continental Underwater Volcanic Eruption and Influence on the Formation of High-Quality Source Rocks: a Case Study of Yingcheng Formation in Xujiaweizi Fault Depression, Songliao Basin. *Sci. China Earth Sci.* 44, 2637–2644.

Song, D. F., He, D. F., Wang, S. R., Li, D., Wang, Z. Y., et al. (2012). Evaluation of Carboniferous Source Rocks in Santanghu Basin. *Xinjiang Pet. Geol.* 3, 305–309.

Taylor, S., McLennan, S. M., Mclennan, J. R., and Hatch, J. S. (1985). The Continental Crust: Its Composition and Evolution Relationship between Inferred Redox Potential of the Depositional Environment and Geochemistry of the Upper Pennsylvanian (Missourian) Stark Shale Member of the Dennis Limestone, Wabaunsee County, Kansas. *U.S.A. Chem. Geol.* 99, 65–82.

Wu, L. G., Li, X. S., Guo, X. B., Luo, Q. S., Liu, X. J., et al. (2012). Diagenetic Evolution and Dissolution Pore Formation Mechanism of Shale Oil Reservoir of Lucaogou Formation in Malang Sag. *J. China Univ. Petroleum* 36, 38–43.

Xie, Z., Yang, C., Li, J., Zhang, L., Guo, J., Jin, H., et al. (2021). Accumulation Characteristics and Large-Medium Gas Reservoir-Forming Mechanism of Tight Sandstone Gas Reservoir in Sichuan Basin, China: Case Study of the Upper Triassic Xujiahe Formation Gas Reservoir. *J. Nat. Gas Geoscience* 6 (5), 269–278. doi:10.1016/j.jnggs.2021.10.001

Xu, Y.-G., Chung, S.-L., Shao, H., and He, B. (2010). Silicic Magmas from the Emeishan Large Igneous Province, Southwest China: Petrogenesis and Their Link with the End-Guadalupian Biological Crisis. *Lithos* 119, 47–60. doi:10.1016/j.lithos.2010.04.013

Xu, Y. G., He, B., Luo, Z. Y., and Liu, H. Q. (2013). Research Progress and Prospect of Igneous Provinces and Mantle Plumes in China. *Bull. mineral rock Geochem.* 32, 25–39.

Xue, P., Zhang, L., Liang, Q., Sun, X., Zhao, Q., and Qi, P. (2020). Thermodynamic Characteristics of CH4 Adsorption by Continental Shale: A Case Study of the Upper Triassic Yanchang Shale in the Yanchang Gasfield, Ordos Basin. *Nat. Gas. Ind. B* 7 (3), 269–277. doi:10.1016/j.ngib.2019.10.009

Yan, J. X., Ma, Z. X., Xie, X. N., Xue, W. Q., Li, B., et al. (2008). Subdivision of Permian Fossil Communities and Habitat Types in Northeast Sichuan, South China. *J. China Univ. Geosciences Engl. Ed.* 19, 441–450. doi:10.1016/S1002-0705(08)60049-7

Yang, W. (2016). *Study on the Evolution and Dynamic Mechanism of Marine Benthic Fauna in the Eastern Sichuan Basin in the Late Permian*. Chengdu: Southwest Petroleum University Press.

Yang, Y., Xie, J., Zhao, L., Huang, P., Zhang, X., Chen, C., et al. (2021). Breakthrough of Natural Gas Exploration in the Beach Facies Porous Dolomite Reservoir of Middle Permian Maokou Formation in the Sichuan Basin and its Implications: A Case Study of the Tridimensional Exploration of Well JT1 in the Central-Northern Sichuan Basin. *Nat. Gas. Ind. B* 8 (4), 393–401. doi:10.1016/j.ngib.2021.07.010

Yin, H. F., and Tong, J. N. (1995). Relationship between Sequence Stratigraphic Boundary and Chronostratigraphic Boundary. *Sci. Bull.* 40, 539–541.

Zhang, W., and Zhang, X. L. (1992). *Permian Reefs and Paleoecology in Southern China*, BeiJing: BeiJing Publishing House, 7, 157.

Zhang, W. Z., Yang, H., Peng, P. A., Yang, Y. H., Zhang, H., et al. (2009). Influence of Late Triassic Volcanic Activity on the Development of Chang 7 High-Quality Source Rocks in Ordos Basin. *J. Geochem.* 38, 573.

Zhou, L., Qian, Y., Zhang, L., Lan, X., Wu, Y., Wang, Q., et al. (2021). Seismic Prediction of Oolitic Beach Thin-Bed Reservoir Based on Favorable Facies Belt Constraints: Taking the Second Member of Feixianguan Formation in Jiulongshan Area, Northwest Sichuan, China. *J. Nat. Gas Geoscience* 6 (6), 329–344. doi:10.1016/j.jnggs.2021.12.002

**Conflict of Interest:** The authors declare that the research was conducted in the absence of any commercial or financial relationships that could be construed as a potential conflict of interest.

**Publisher's Note:** All claims expressed in this article are solely those of the authors and do not necessarily represent those of their affiliated organizations, or those of the publisher, the editors, and the reviewers. Any product that may be evaluated in this article, or claim that may be made by its manufacturer, is not guaranteed or endorsed by the publisher.